An effective surface-enhanced Raman scattering template based on gold nanoparticle/silicon nanowire arrays*

Wang Ming-Li(王明利)[a], Zhang Chang-Xing(张常兴)[b], Wu Zheng-Long(吴正龙)[c], Jing Xi-Li(井西利)[a]†, and Xu Hai-Jun(许海军)[b]‡

[a] College of Sciences, Yanshan University, Qinhuangdao 066004, China
[b] School of Science and State Key Laboratory of Chemical Resource Engineering, Beijing University of Chemical Technology, Beijing 100029, China
[c] Analytical and Testing Center, Beijing Normal University, Beijing 100875, China

(Received 24 November 2013; revised manuscript received 8 February 2014; published online 20 April 2014)

A large-scale Si nanowire array (SiNWA) is fabricated with gold (Au) nanoparticles by simple metal-assisted chemical etching and metal reduction processes. The three-dimensional nanostructured Au/SiNWA is evaluated as an active substrate for surface-enhanced Raman scattering (SERS). The results show that the detection limit for rhodamine 6G is as low as 10^{-7} M, and the Raman enhancement factor is as large as 10^5 with a relative standard deviation of less than 25%. After the calibration of the Raman peak intensities of rhodamine 6G and thiram, organic molecules could be quantitatively detected. These results indicate that Au/SiNWA is a promising SERS-active substrate for the detection of biomolecules present in low concentrations. Our findings are an important advance in SERS substrates to allow fast and quantitative detection of trace organic contaminants.

Keywords: surface-enhanced Raman scattering, nanowire array, quantitative detection

PACS: 78.30.–j, 74.25.nd, 61.46.–w **DOI:** 10.1088/1674-1056/23/6/067802

1. Introduction

Surface-enhanced Raman scattering (SERS) has attracted much attention because of its high sensitivity and potential application in chemical and biomedical analysis.[1–4] Raman signal enhancement of the order of 10^8–10^{14} can be achieved by SERS, and it has the unique ability to recognize an analyte at a very low concentration in aqueous solution. These merits make SERS a unique technology for ultrasensitive biological and chemical analysis and environmental sensing.[5–10] In addition, another important feature of SERS is that a high level of detection selectivity can be achieved by controlling the chemical properties around the metal surface. SERS can detect a single species in a complex mixture in a wide range from a nano- to micro-molar level.[3,7–12] Because of the high selectivity and sensitivity of SERS as well as the highly informative characteristics of Raman spectroscopy, SERS has become an increasingly more common and feasible alternative to other optical methods. The enhancement effects observed in SERS have been attributed to two models, i.e., the chemical mechanism and the electromagnetic mechanism (EM).[13] The EM, which results from an increased local electromagnetic field (hot spot) at a metallic nanoparticle (NP) surface arising from the interaction of the incident laser with the electrons of the metallic surface, is the commonly accepted origin of SERS.[14] At present, surface plasmon resonance (SPR) is believed to be the major contribution to electromagnetic enhancement, so many researchers have fabricated various metal colloids to examine the function of SPR.[15,16] For wide application of SERS, an effective substrate needs to be developed.[17] An ideal substrate should possess excellent stability, repeatability, low cost, and also should be easy to fabricate and handle. Various methods to fabricate SERS substrates have been developed to date. For example, pure metal may be used as the material to fabricate SERS substrates, which can be fashioned into NPs,[18] nanorods,[19,20] nanowires (NWs),[21,22] nanoflowers,[23] core–shell structure, and nanofilms.[24,25] These materials are fabricated by methods including vapor–liquid–solid growth,[26] thermal evaporation decomposition,[27] supercritical fluid–liquid–solid synthesis,[28] molecular beam epitaxy,[29] solution growth, and template-based lithography.[30,31] Although these preparation methods can readily produce functional SERS substrates, the procedures are complicated and expensive, which limits batch production on a large scale. Recently, metal-assisted etching of silicon wafers to produce nanowires at room temperature has attracted widespread interest.[32,33] Considering that the reductive nature of silicon (Si) substrate could effectively improve the long-term stability of SERS substrate by inhibiting noble metal oxidization, and the noble metal silver (Ag) is one of the best materials for making SERS-

*Project supported by the National Natural Science Foundation of China (Grant No. 11104008), the Beijing Natural Science Foundation, China (Grant No. 4142040), the Doctoral Fund of the Ministry of Education of China (Grant No. 20090010120014), the Beijing Higher Education Young Elite Teacher Project, and the Technology Research and Development Program of Qinhuangdao City, China (Grant Nos. 201001A034 and 2012021A056).

†Corresponding author. E-mail: jingxili@ysu.edu.cn
‡Corresponding author. E-mail: hjxu@mail.buct.edu.cn

© 2014 Chinese Physical Society and IOP Publishing Ltd

active surfaces, the simple preparation of Ag/Si nanostructured arrays each with long-term stability and high sensitivity is highly desirable.[34–36] Unfortunately, such structures are unstable and readily oxidized under ambient conditions. An alternative to Ag is gold (Au), which possesses not only high stability in the atmosphere, but also strong SERS activity in the visible light wavelength region. Au-prepared Si NW array (SiNWA) nanostructures are therefore excellent candidates for molecular sensing with high SERS sensitivity, reproducibility, and stability. Therefore, we combine Au NPs with SiNWAs to produce SERS-active substrates.

In this paper, Au/SiNWA substrates are fabricated in three steps by noble metal-assisted chemical etching. Rhodamine 6G (R6G) is used to characterize the SERS performances of the substrates, including uniformity and sensitivity. The results indicate that each of the substrates possesses good uniformity with a relative standard deviation (RSD) of less than 0.25. Simultaneously, a detection level as low as 10^{-8} M is achieved, which is sufficient for practical application.

2. Experiments

N-type (100) Si wafers (1 Ω·cm–10 Ω·cm) purchased from the Tianjin Semiconductor Technology Research Institute were used as the substrate material. Acetone, alcohol, HF ($\geq$ 40%), H_2O_2 (30%), nitric acid (98%), sodium hydroxide, silver nitrate, and deionized water were purchased from the Beijing Chemical Works. $HAuCl_4{\cdot}3H_2O$, R6G, and thiram were obtained from Aladdin. First, a Si wafer was cut into dimensions of 1 cm×3 cm. The cut Si wafer was sequentially cleaned in water, acetone, and alcohol for 5 min each. The clean Si wafer was then dried in air. The wafer was placed in a mixture of 4.6-M HF and 0.005-M $AgNO_3$ for 1 min, and then washed with deionized water multiple times to remove excess Ag particles. Ag NPs were then deposited on the surface of the Si wafer by placing the wafer in a mixture 4.6-M HF and 0.5-M H_2O_2 at room temperature for 60 min.

In the procedure used to prepare the SiNWAs, Ag was used as an assistant material, but the final aim of the experiment was to form a Au/Si composite structure. Therefore, the formed SiNWAs were immersed in nitric acid (48%) for 10 min to remove the Ag NPs. However, this method of removing Ag could result in the nitric acid oxidizing the Si. Therefore, SiNWAs immersed in nitric acid solution were then placed in HF (98%) for 10 min to eliminate any possible oxidation of silica. The SiNWAs were now ready for the next procedure.

$HAuCl_4.3H_2O$ (1 M) and methanol (3 mL) were added to water (50 mL). Sodium hydroxide solution was added dropwise until the pH of the solution was 7–8. The SiNWAs were added to this slowly stirred solution, which was then heated and maintained at 120 °C for 2 h. A solution of R6G (10^{-3} M) and other prepared solutions were successively diluted by a factor of 10 to give a final concentration of 10^{-9} M. Thiram is poorly soluble in water. Therefore, we dissolved thiram in alcohol to give a solution with a concentration of 10^{-3} M. Solutions of thiram with a concentration of 10^{-4}–10^{-9} could be obtained via the above dilution method with deionized water.

The morphology, microstructure, and chemical composition of the as-fabricated SiNWAs and Au/SiNWAs were characterized by field-emission scanning electron microscopy (FE-SEM) (JEOL JSM-6700F) with energy-dispersive spectroscopy (EDS) and x-ray diffraction (XRD) (Rigaku Ultima III). SERS measurements were performed at room temperature on a LabRAM ARAMIS Raman system using a 632.8-nm helium–neon laser line for excitation. The laser spot size was $\sim$ 1 μm with an incident power of 0.325 mW and acquisition time of 24 s. The same accumulation times and laser power were used to obtain all Raman spectra.

3. Results and discussion

Figure 1 shows the top and cross-sectional FE-SEM images of SiNWA and Au/SiNWA, which clearly show that Au NPs are successfully deposited on the surface of the SiNWA. Comparing the enlarged images in the insets of Figs. 1(a) and 1(c) further confirms that Au NPs are present on the SiNWA surface. Figures 1(b) and 1(e) show the cross-sectional images of the SiNWA and Au/SiNWA, which reveal that the diameters and lengths of the SiNWs are about 100 nm–500 nm and their lengths are all 35 μm, and the average distance between SiNWs is $\sim$ 200 nm. The SiNWs are well aligned over a large area. The top-view FE-SEM images indicate that the diameters of Au NPs range from 100 nm to 400 nm, with an average diameter of approximately 150 nm, and Au NPs are stacked in layers on the Si NWs. Judging from the inset in Fig. 1(c) and magnified image in Fig. 1(d), the diameters of Au NPs on the sidewalls of SiNWs are much smaller than those on the top of Si NWs. Moreover, Au NPs only cover the upper half of each Si NW, which is further confirmed by EDS analysis. As shown in Table 1, the atomic percentages of Au are greatly different in the four different areas of the Au/SiNWA. This phenomenon could be explained by the structure of the Si substrate as follows. At the beginning of the Au reduction process, the Au NPs are small and can enter into the gaps between SiNWs and adsorb onto their surface. However, the Au NPs readily coalesce, which will lead to the formation of the layered structure of most of the NPs on the top of the SiNWs. At this point, few Au NPs could enter into the gaps between SiNWs. Furthermore, the coalescence of Au NPs would fill the gap between SiNWs, which further restricts the formation of Au NPs on the surface of SiNWs. The SiNWs are about 35-μm long, so they are unable to be covered entirely by the Au NPs.

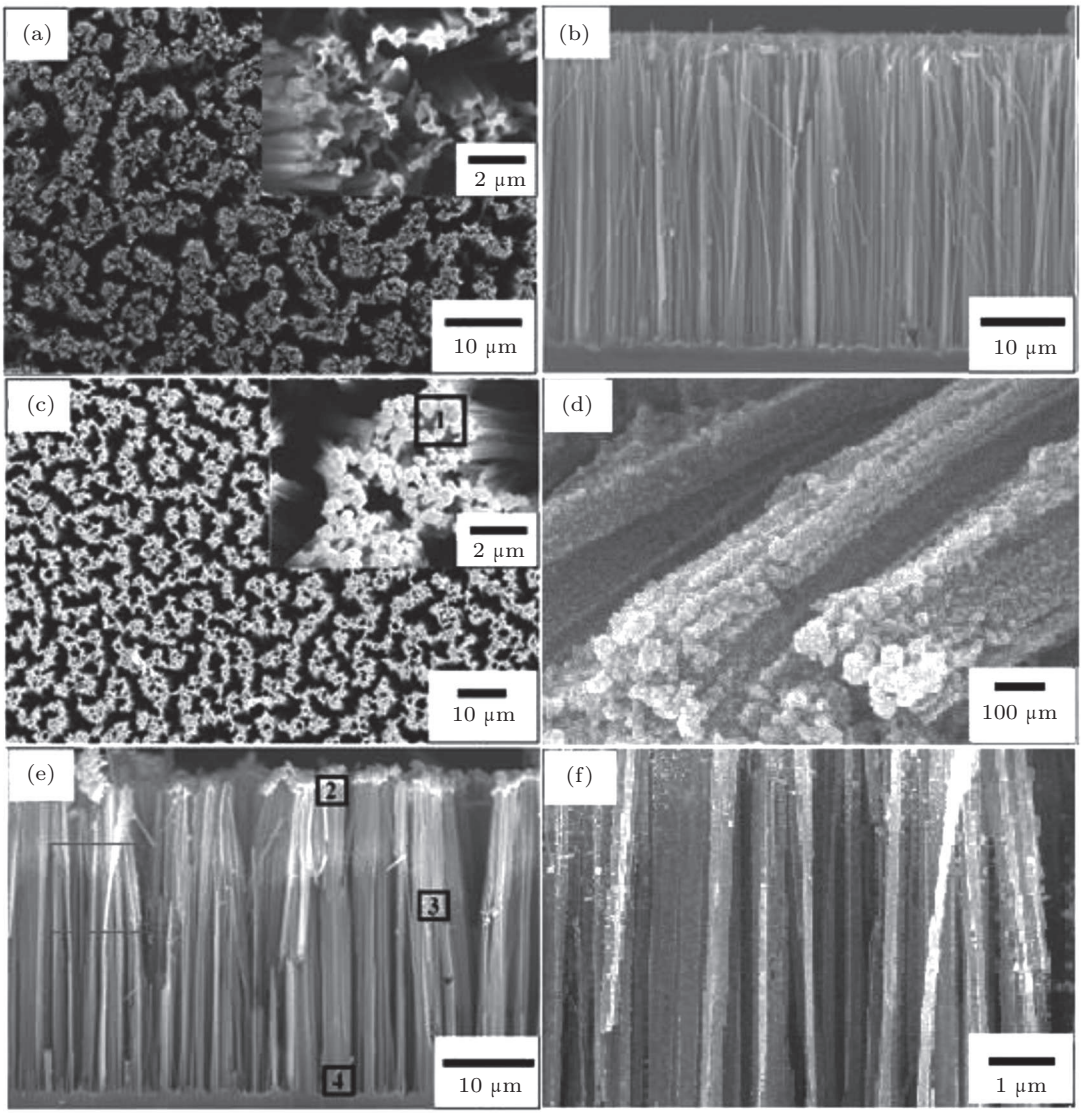


Fig. 1. FE-SEM images of the SiNWA and Au/SiNWA. Panels (a) and (b) show the typical top and cross-sectional views of the SiNWA, panels (c) and (d) show the top views of the Au/SiNWA at different magnifications, panels (e) and (f) show the cross-sectional views of the Au/SiNWA at different magnifications, and panel (f) shows a magnified image of panel (e). Insets in panels (a) and (c) show locally magnified FE-SEM images.

Table 1. Atomic percentages of Si, Au, and O in different areas of an Au/SiNWA.

	Si	Au	O
Zone 1	34.25	60.99	4.76
Zone 2	78.51	2.94	18.55
Zone 3	81.79	0.93	17.28
Zone 4	85.05	0.00	14.95

A crystal of the Au/SiNWA is investigated by XRD analysis. Figure 2 shows that the SiNWA is crystalline with a major (400) diffraction peak, which confirms that Si has a (400) growth direction. Moreover, all spectra show two sets of diffraction peaks, indicating that synthesized products are all composite materials. The peaks marked with Si (400) can be indexed to the diamond structure of Si, while the remainder can be indexed to the face-centered-cubic structure of Au. No other crystalline impurities are observed.

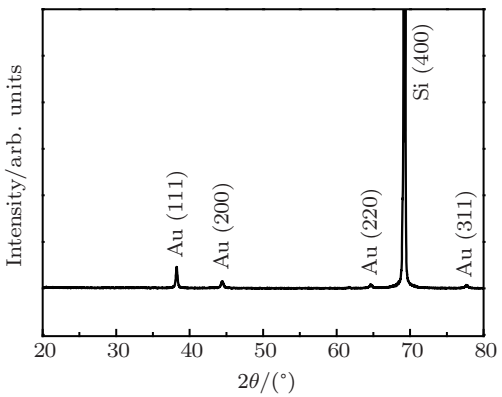


Fig. 2. XRD image of the Au/SiNWA composite structure.

The ability for Au/SiNWA to enhance the Raman signal of analytes is investigated using R6G as the probe molecule. R6G has been used extensively for SERS studies since the early development of this technique and has well-established vibration features. Figure 3(a) shows the SERS of different

concentrations of R6G solution dispersed on the Au/SiNWA in a range of 10^{-3} M–10^{-7} M. The SERS detection level of R6G for Au/SiNWA is 10^{-7} M. Because the SERS of Si is very strong, which seriously affects the results obtained for solutions with low concentrations, the second peak of Si between 900 cm^{-1} and 1050 cm^{-1} is eliminated. The strong and medium-strong Raman bands at 612, 775, 1189, 1311, 1361, 1508, 1571, and 1646 cm^{-1} are assigned to carbon ring vibration, ethylamine group wagging, and carbon–oxygen stretching of the R6G molecule.[37] To investigate the change of Raman spectrum of R6G with its concentration, the Raman spectrum is fitted and a curve showing the logarithmic relationship between the area of the peak around 612 cm^{-1} and concentration is obtained, which is presented in Fig. 3(b). The curve is close to a straight line, indicating that the Raman signal strength increases proportionally with concentration increasing.

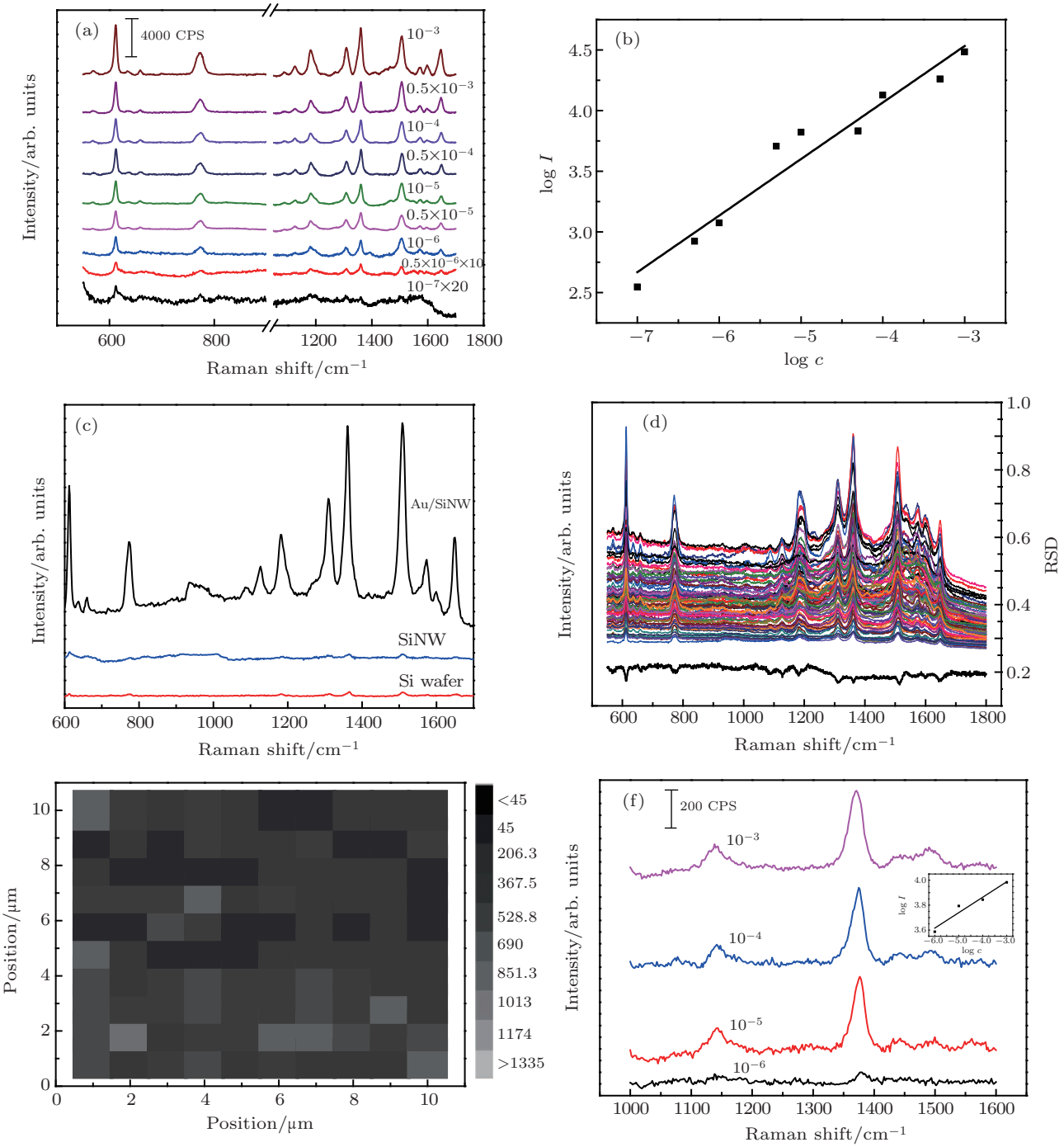


Fig. 3. (color online) (a) SERS of R6G solutions with concentrations of 10^{-3} M–10^{-7} M with Au/SiNWA, (b) quantitative relation between the SERS band at 612 cm^{-1} and concentration, (c) SERS of 10^{-3} M R6G on three different substrates: Si wafer, SiNWA, and Au/SiNWA, (d) SERS of 10^{-5} M R6G at 100 different points on the Au/SiNWA; the RSD is less than 0.25, (e) SERS mapping (step size = 3 μm, 10×10 = 100) of the Au/SiNWA substrate, and (f) SERS of thiram with concentrations of 10^{-3} M–10^{-6} M on a Au/SiNWA. The inset image is the quantitative relation between the SERS band at 1380 cm^{-1} and concentration.

To understand the ability for the Au/SiNWA composite structure to enhance the Raman signal, several tests are carried out using three different substrates to detect 10^{-3} M R6G. To determine the enhancement factor (EF) of the Au/SiNWA composite structure, a Si substrate without Au NPs is used as a reference along with the following standard equation:[38] EF=$(I_{\rm SERS}/I_{\rm Raman})\times(N_{\rm Raman}/N_{\rm SERS})$, where $I_{\rm SERS}$ and $I_{\rm Raman}$ are the integrated Raman intensities of a specific SERS peak observed for the solutions adsorbed on Au/SiNWA and SiNWA, respectively; $N_{\rm SERS}$ and $N_{\rm Raman}$ are the numbers of molecules adsorbed on the surface of the corresponding substrates. Figure 3(c) shows the results of this experiment, which indicate that the enhancement of the planar Si wafer is close to that of the SiNWA, where the relative intensities of the Raman signal at 1361 $\rm cm^{-1}$ are 76 and 92, respectively. There is a marked change of the intensity of Raman peak at 1380 $\rm cm^{-1}$ using the Au/SiNWA substrate, with the relative intensity reaching about 3000. Therefore, the calculated values in intensities from Au/SiNWA to SiNWA are about 32.6 (3000/92). Considering that $N_{\rm SERS}$ and $N_{\rm Raman}$ are mainly determined by the concentrations of molecules in a given volume and area, and the surface geometries of Au/SiNWA and SiNWA are also similar, it is reasonable to say that the ratio of R6G concentrations is a reasonable estimation of the ratio of $N_{\rm Raman}$ to $N_{\rm SERS}$. As a result, $N_{\rm Raman}/N_{\rm SERS}$ is about 10^4. Therefore, the EF of Au/SiNWA is as high as 3.26×10^5, which is about ten times higher than the values reported elsewhere.[39–41] The marked Raman enhancement of organic molecules is mainly attributed to the Au/SiNWA possessing two kinds of hot spots, one is on the side surface of the same NW and the other is on the side surface of two neighboring NWs. The high density of hot spots on the sidewall of the SiNWA may also increase the number of adsorbed probe molecules within a detection volume, which further enhances the Raman signal. These features make the Au/SiNWA a promising material to be used as a substrate for SERS.

According to the above analyses of the morphology and structure of the Au/SiNWA, some following factors may contribute to the strong local electromagnetic field that results in strong Raman enhancement. (i) The Au/SiNWA is of a three-dimensional (3D) structure, so the SiNWs could provide a large surface area to adsorb Au NPs compared with a traditional planar structure, so more analytes can combine with the substrate.[42] (ii) The length of each Si NW is about 35 μm (Fig. 1(c)). Meanwhile, a great number of Au NPs are deposited on the surface of the Si NWs. These Au NPs would be captured if the excitation light enters into the gap between Si NWs, increasing the interactions of the light with Au NPs. Light could be scattered multiple times between Au NPs, which will improve the use of excitation light and enhance the local field. (iii) The distance between Au NPs is short, which facilitates the formation of hot spots. It has been shown that the spaces between metallic particles can act as hot spots where the intensity of the optical field is much higher than at other sites. This results in a strong Raman signal from locally adsorbed probe molecules.[42–44] For example, it has been theoretically demonstrated that the effective Raman cross section for a molecule placed between two metal NPs can be enhanced by more than 7–12 orders of magnitude because of the strong electromagnetic coupling between two adjacent metallic objects. This enhancement dominates the SERS response in nanostructure arrays.[42,43,45] Several theoretical calculations have also confirmed that the field enhancement originating from gaps between NPs play an important role in SERS.[44,46] For instance, Choi *et al.*[47] suggested that higher SERS enhancement for metal NPs could be achieved by restricting the gap between them to less than 30 nm. The signal enhancement arises from not only the local electromagnetic effect of Au NPs on a single Si NW, but also that between Si NWs. (iv) Besides these geometrical features, the interactions between Au and Si can also contribute to the increase in EF through the excitation of surface plasmons in the metal.

Figures 3(d) and 3(e) display the uniformity of Au/SiNWA substrate via mapping of 10^{-5} M R6G. One hundred points are selected in a rectangular area of the substrate to detect the signal from R6G, and the RSD of each data point for these 100 randomly selected positions is calculated using the same Raman band as shown in Fig. 3(d). In this case, the RSD values of the signal intensities of major SERS peaks for 10^{-5} M R6G are all below 0.25, and the intensities of the peaks are similar to those at the other points. This conclusion is further confirmed in Fig. 3(e), in which the brightness of the rectangular region is proportional to the signal integral intensity centered at 612 $\rm cm^{-1}$. It is obvious that the brightness is close to each other, which indicates that the uniformity of the Au/SiNWA substrate is good to some extent over its entire area.[48]

Food safety has attracted wide concern in recent years, especially the effects that pesticide residues have on the human body. Traditional methods of testing pesticide residues in food are time consuming, and the available resources and detection limit are not satisfactory. SERS is a favorable method for this usage because of advantages including rapid response, nondestructive nature, trace detection limit, and easy operation. Thiram is commonly used as a seed dressing, and is present as a trace residue in crops. Theoretically, the C=S and S–S bonds in thiram will break when it reacts with a metal.[49] Then, two Au–S bond are formed, which are easy to detect by SERS. Therefore, we decide to detect thiram using the Au/SiNWA substrate. The results of this experiment are shown in Fig. 3(f). A detection limit of 10^{-6} M is achieved. The Raman spectrum is also fitted and a curve of the logarithmic relation-

ship between the area of peak at 1380 cm^{-1} and concentration is obtained (see the inset in Fig. 3(f)). This curve is close to a straight line, indicating that the Raman signal strength increases proportionally with concentration increasing. The ability for Au NPs to enhance the Raman signal is sufficient for practical applications.

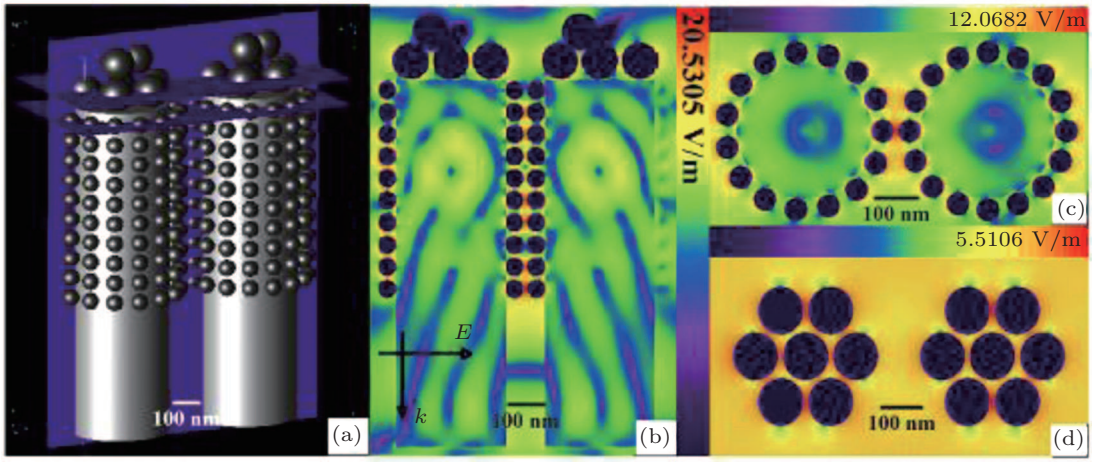


Fig. 4. (color online) Simulation of the EM field distribution in a model of the Au/SiNWA using 3D finite-difference time domain software. Here, the polarization of incident light is indicated by arrows. Panel (a) shows the shape of the model Au/SiNWA nanostructure and the wave vector; panels (b), (c), and (d) show the calculated spatial distributions of the electric field intensity for the vertical, middle, and top horizontal planes, respectively.

To better understand these experimental results, a 3D finite-difference time domain (3D-FDTD) software is used to simulate a model of the Au/SiNWA to further investigate the mechanism of SERS following excitation at $\lambda = 633$ nm. The essence of the FDTD method is to solve the Maxwell equations to determine the space distribution of an electromagnetic field as a function of time. To accord with the actual structure of the Au/SiNWA, the model is built on the basis of the SEM images in Figs. 1(b) and 1(d). The final structure is shown in Fig. 4(a), in which the average diameters of Si NW are both ~ 300 nm and the gap between them is $\sim$120 nm. Au and NPs are overlapping on the top of the Si and NWs and their diameters are in a range of 100 nm–400 nm as shown in the top-view SEM image in Fig. 1(b). We must use Si NWs with a length of 1000 nm because of the computation limitation of the computer hardware. Figures 4(b)–4(d) show the E-field distributions around the Au/Si nanostructures excited at $\lambda = 633$ nm, and the orientation and polarization of the excitation light are also indicated. The maximum electric field intensity is about 20.5 V/m and the corresponding EF is approximately 10^5. This theoretical calculation result is smaller than the value obtained experimentally, which is attributed to the following causes. Only two Si NWs are simulated, and the Au NPs on the surface of one Si NW only interact with those on the other. However, they will also be affected by the Si NWs around them, so a higher electromagnetic field will be obtained in the actual arrays. In addition, Au NPs are ordered in this model, with a smooth surface. These characteristics do not correspond with the actual situation. Overall, these discrepancies result in the difference between theoretical and experimental EF for the Au/SiNWA.

4. Conclusions

In this paper, vertically aligned Au/SiNWA that generates high-density SERS hot spots within a detection volume is fabricated by a simple, inexpensive method. This 3D SERS substrate yields extremely high SERS activity with a calculated EF of up to 10^5 and detection limits of 10^{-7} M for R6G and 10^{-6} M for thiram. The linear dependence of the logarithmic integrated intensity on the logarithmic concentration of the target molecules provides a new method of rapidly and quantitatively detecting organic molecules. Moreover, the enhancement mechanism of the Au/SiNWA is examined in detail. 3D-FDTD simulations confirm the authenticity of experimental results. This fabrication strategy, which is compatible with well-established Si technology, may be easily integrated into lab-on-chip sensing devices for label-free chemical/biomolecule detection.

References

[1] Bell S E J and Sirimuthu N M S 2006 *J. Am. Chem. Soc.* **128** 15580
[2] Xie W, Walkenfort B and Schlucker S 2013 *J. Am. Chem. Soc.* **135** 1657
[3] Nie S M and Emory S R 1997 *Science* **275** 1102
[4] Sackmann M and Materny A 2006 *J. Raman Spectrosc.* **37** 305
[5] Moskovits M 1985 *Rev. Mod. Phys.* **57** 783
[6] Zheng J, Jiao A L, Yang R H, Li H M, Li J S, Shi M L, Ma C, Jiang Y, Deng L and Tan W H 2012 *J. Am. Chem. Soc.* **134** 19957
[7] Camden J A, Dieringer J A, Wang Y, Masiello D J, Marks L D, Schatz G C and Van D R P 2008 *J. Am. Chem. Soc.* **130** 12616

[8] Guo H Y, Jiang D, L H B, Xu S P and Xu W Q 2013 *J. Phys. Chem. C* **117** 564
[9] Barhoumi A, Zhang D, Tam F and Halas N J 2008 *J. Am. Chem. Soc.* **130** 5523
[10] Qian X M, Li J and Nie S M 2009 *J. Am. Chem. Soc.* **131** 7540
[11] Tiwari V S, Tovmachenko O, Darbha G K, Hardy W, Singh J P and Ray P C 2007 *Chem. Phys. Lett.* **446** 77
[12] Hutchison J A, Centeno S P, Odaka H, Fukumura H, Hofkens J and Hiroshi U I 2009 *Nano Lett.* **9** 995
[13] Campion A and Kambhampati P 1998 *Chem. Soc. Rev.* **27** 241
[14] Esenturk E N and Walker A R H 2009 *J. Raman Spectrosc.* **40** 86
[15] Lin X M, Cui Y, Xu Y H, Ren B and Tian Z Q 2009 *Anal. Bioanal. Chem.* **394** 1729
[16] Grzelczak M, Perez J J, Mulvaney P and Liz M L M 2008 *Chem. Soc. Rev.* **37** 1783
[17] Natan M J 2006 *Faraday Discuss.* **132** 321
[18] Samuel S R D, Singh A K, Dulal S, Yu H T and Paresh C R 2009 *J. Am. Chem. Soc.* **131** 13806
[19] Shi X Z, Shen C M, Wang D K, Li C, Tian Y, Xu Z C, Wang C M and Gao H J 2011 *Chin. Phys. B* **20** 076103
[20] Liu Y J, Chu H Y and Zhao Y P 2010 *J. Phys. Chem. C* **114** 8176
[21] Hsiao W H, Chen H Y, Yang Y C, Chen Y L, Lee C Y and Chiu H T 2011 *ACS Appl. Mate. Interfaces* **3** 3280
[22] Deng C Y, Zhang G L, Zou B, Shi H L, Liang Y J, Li Y C, Fu J X and Wang W Z 2013 *Chin. Phys. B* **22** 106102
[23] Jena B K and Raj C R 2008 *Chem. Mater.* **20** 3546
[24] Li J F, Huang Y F, Ding Y, Yang Z L, Zhou X S, Fan F R, Zhang W, Zhou Z Y, Wu D Y, Ren B, Wang Z L and Tian Z Q 2010 *Nature* **464** 392
[25] Liu R, Liu J F, Zhou X X, Sun M T and Jiang G B 2011 *Anal. Chem.* **83** 9131
[26] Lerose D, Bechelany M, Philippe L, Michler J and Christiansen S 2010 *J. Cryst. Growth* **312** 2887
[27] Pan H, Lim S, Poh C, Sun H, Wu X, Feng Y and Lin J 2005 *Nanotechnology* **16** 417
[28] Yuan F W and Tuan H Y 2010 *Cryst. Growth Des.* **10** 4741
[29] Shao M W, Ma D D and Lee S T 2010 *Eur. J. Inorg. Chem.* **2010** 4264
[30] Chun J Y and Lee J W 2010 *Eur. J. Inorg. Chem.* **27** 4251
[31] Yang Y H, Wu S J, Chiu H S, Lin P I and Chen Y T 2004 *J. Phys. Chem. B* **108** 846
[32] Li X and Bohn P W 2000 *Appl. Phys. Lett.* **77** 2572
[33] Zhang M L, Peng K Q, Fan X, Jie J S, Zhang R Q, Lee S T and Wong N B 2008 *J. Phys. Chem. C* **112** 4444
[34] Saito Y, Wang J J, Smith D A and Batchelder D N 2002 *Langmuir.* **18** 2959
[35] Huo S J, Xue X K, Li Q X, Xu S F and Cai W B 2006 *J. Phys. Chem. B* **110** 25721
[36] Fang C, Agarwal A, Widjaja E, Garland M V, Wong S M, Linn L, Khalid N M, Salim S M and Balasubramanian N 2009 *Chem. Mater.* **21** 3542
[37] Hildebrandt P and Stockburger M 1984 *J. Phys. Chem.* **88** 5935
[38] Wang X T, Shi W S, She G W, Mu L X and Lee S T 2010 *Appl. Phys. Lett.* **96** 053104
[39] Shen J H, Zhu Y H, Yang X L, Zong J and Li C Z 2013 *Langmuir.* **29** 690
[40] Hong J W, Lee S U, Lee Y W and Han S W 2012 *J. Am. Chem. Soc.* **134** 4565
[41] Li L, Hutter T, Finnemore A S, Huang F M, Baumberg J J, Stephen R E, Steiner U and Mahajan S 2012 *Nano Lett.* **12** 4242
[42] Vidal F J G and Pendry J B 1996 *Phys. Rev. Lett.* **77** 1163
[43] Xu H X, Aizpurua J, Kall M and Apell P 2000 *Phys. Rev. E* **62** 4318
[44] Fang J X, Yi Y, Ding B J and Song X P 2008 *Appl. Phys. Lett.* **92** 131115
[45] Qiu T, Zhou Y J, Li J Q, Zhang W J, Lang X Z, Cui T J and Chu P K 2009 *J. Phys. D: Appl. Phys.* **42** 175403
[46] Qin L D, Zou S L, Xue C, Atkinson A, Schatz G C and Mirkin C A 2006 *Proc. Natl. Acad. Sci. USA* **103** 13300
[47] Choi C J, Xu Z D, Wu H Y, Liu G L and Cunningham B T 2010 *Nanotechnology* **21** 415301
[48] Zhang B H, Wang H S, Lu L H, Ai K L, Zhang G and Cheng X L 2008 *Adv. Funct. Mater.* **18** 2348
[49] Sánchez Corte's S, Domingo C, García Ramos J V and Aznárez J A 2001 *Langmuir.* **17** 1157